Mon. Not. R. Astron. Soc. **000**, 000–000 (0000) Printed 4 October 2013 (MN LATEX style file v2.2)

SRG/eROSITA prospects for the detection of stellar tidal disruption flares

I. Khabibullin[1,2⋆], S. Sazonov[1,3,2] and R. Sunyaev[2,1]
[1]*Space Research Institute, Russian Academy of Sciences, Profsoyuznaya 84/32, 117997 Moscow, Russia*
[2]*Max-Planck-Institut für Astrophysik, Karl-Schwarzschild-Str. 1, 85740 Garching bei München, Germany*
[3]*Moscow Institute of Physics and Technology, Institutsky per. 9, 141700 Dolgoprudny, Russia*

4 October 2013

ABSTRACT

We discuss the potential of the eROSITA telescope on board the *Spectrum-Roentgen-Gamma (SRG)* observatory to detect stellar tidal disruption events (TDE) during its 4-year all-sky survey. These events are expected to reveal themselves as luminous flares of UV/soft X-ray emission associated with the centers of previously non-active galaxies and fading by few orders of magnitude on time-scales of several months to years. Given that eROSITA will complete an all-sky survey every 6 months and a total of 8 such scans will be performed over the course of the mission, we propose to distinguish TDEs from other X-ray transients using two criteria: i) large (more than a factor of 10) X-ray variation between two subsequent 6-month scans and ii) soft X-ray spectrum. The expected number of TDE candidates is $\sim 10^3$ per scan (with most of the events being new discoveries in a given scan), so that a total of several thousand TDE candidates could be found during the 4-year survey. The actual number may significantly differ from this estimate, since it is based on just a few TDEs observed so far. The eROSITA all-sky survey is expected to be nearly equally sensitive to TDEs occurring near supermassive black holes (SMBH) of mass between $\sim 10^6$ and $\sim 10^7 M_\odot$ and will thus provide a unique census of quiescent SMBHs and associated nuclear stellar cusps in the local Universe ($z \lesssim 0.15$). Information on TDE candidates will be available within a day after their detection and localization by eROSITA, making possible follow-up observations that may reveal peculiar types of TDEs.

1 INTRODUCTION

It is widely accepted that supermassive black holes (SMBH), i.e. black holes with mass of hundreds of thousands to billions of solar masses, reside in the centers of most galaxies (see Ho 2008 for a review). However, apart from active galactic nuclei (AGN), where intense accretion of gas onto the SMBH takes place, and the nuclei of the few most nearby optically non-active galaxies, where dynamics of stars and gas near the SMBH can be directly measured, such black holes remain hidden (Kormendy & Richstone 1995; Kormendy, Ho 2001). A plausible scenario for revealing a compact object with $M \lesssim 10^8 M_\odot$[1] in the center of an inactive galaxy is based on tidal disruption of stars passing sufficiently close to it (Hills 1975; Lidskii & Ozernoi 1979). According to analytical estimates, about half of the disrupted star's material should be captured and then accreted by the SMBH on a time-scale of about a year (Gurzadian & Ozernoi 1981; Rees 1988). Numerical simulations confirm these suggestions (Evans & Kochanek 1989; Laguna et al. 1993), though Ayal, Livio, & Piran (2000) found that only about 10% of the original star's mass actually gets accreted. Accretion of the stellar debris onto a SMBH gives rise to a flare of thermal radiation with the peak at extreme ultraviolet (EUV)/soft X-ray wavelengths and maximum luminosity of 10^{43} – 10^{45} erg s^{-1}(Strubbe & Quataert 2009). However, the expected rate of such tidal disruption events (TDE) is not high: depending on the stellar density in the nuclear cusp and the SMBH mass, it varies from 10^{-6} to 10^{-3} yr^{-1} per galaxy (Wang & Merritt 2004). Consistent with these expectations, just about a dozen of TDE candidates have been identified so far by X-ray (Komossa 2002; Donley et al. 2002; Esquej et al. 2008; Cappelluti et al. 2009; Maksym, Ulmer, & Eracleous 2010; Lin et al. 2011; Saxton et al. 2012), UV (Gezari et al. 2009 and references therein) and optical (van Velzen et al. 2011b and references therein) observations. The observed spectral and temporal properties of these TDE candidates support the general picture of captured stellar debris forming an accretion disk around a SMBH, but the existing data are too sparse to provide stringent constraints on the theoretical models.

Recently, it has also been recognized that powerful jets could emerge during accretion of stellar debris onto a SMBH, giving rise to radio and hard X-ray emission (Giannios & Metzger 2011; van Velzen, Körding, & Falcke 2011; Lei & Zhang 2011; Krolik & Piran 2012). The subsequent discovery by *Swift* of TDE candidates that fit well into this scenario (Levan et al. 2011; Burrows et al. 2011; Cenko et al. 2012) opened an extra dimension

[1] SMBHs with $M \gtrsim 10^8 M_\odot$ are expected to capture solar-type stars without disruption, since the corresponding tidal radius is smaller than the radius of the black hole's event horizon. Also, in the situation where the tidal and horizon radii are close to each other, general relativity effects cause the capture probability to strongly depend on the black hole spin (Kesden 2012).

in TDE studies. It is currently unclear whether the observed rarity of such flares is owing to a high degree of jet collimation or to a low intrinsic probability of jet production (Cenko et al. 2012). Obviously, a larger sample of TDEs is needed to check the different possibilities and test the existing theoretical models.

Deep wide-area surveys are especially powerful in discovering transient sources, usually by comparison with pre- or post-survey observations. As regards giant thermal flares from stellar TDEs, EUV/soft X-ray surveys are the most suitable. Up to several thousand TDEs had been expected to be detected during the *ROSAT* All-Sky Survey (RASS, Sembay & West 1993), but only *five* were actually identified due to the lack of timely follow-up observations and deep X-ray observations to confirm the pre- or post-outburst state (Komossa 2002; Donley et al. 2002). Nonetheless, the RASS has provided the largest contribution to the existing sample of X-ray TDE detections. The several other candidates have been found in the *XMM-Newton* Slew Survey (Esquej et al. 2008; Lin et al. 2011; Saxton et al. 2012) and in *Chandra* pointed observations (Cappelluti et al. 2009; Maksym, Ulmer, & Eracleous 2010).

In the present paper, we investigate opportunities provided by the upcoming *Spectrum-X-Gamma (SRG)* mission. This observatory is planned to be launched in 2014 to the L2 point of the Earth–Sun system and the first 4 years of the mission will be devoted to an all-sky survey in the 0.2–12 keV energy band with the eROSITA[2] (Merloni et al. 2012) and ART-XC[3] (Pavlinsky et al. 2012) telescopes. The survey will consist of 8 repeated half-a-year scans of the entire sky, each with sensitivity (below 2 keV) $\sim$ 4 times better than RASS. Owing to this observational strategy, 'self-follow-up' observations of X-ray sources will be possible through scan-to-scan comparison. As one of the main TDE hallmarks is a giant amplitude of flux variations on the time-scale of years, searches for such events in the eROSITA All-Sky Survey (eRASS) data can be very efficient (see Fig. 1). An additional identification tool will be provided by X-ray spectral analysis, taking advantage of the high sensitivity in the 0.2–2 keV energy range and the possibility of detection of harder photons with energies up to $\sim$ 10 keV. Below, after a short overview of TDE X-ray emission properties, we specify the required identification criteria and estimate the expected TDE detection rate for eRASS.

2 X-RAY SIGNATURES OF TIDAL DISRUPTION EVENTS

The observational appearance of a given TDE may depend on the properties of the star (mass and type) and SMBH (mass and spin) as well as on the initial stellar orbit characteristics. To simplify the treatment, we shall use some 'average' pattern which is based on the standard theory of tidal disruption of a *Sun-like* star and which satisfactorily reflects major observational properties of the currently available sample of X-ray selected TDEs. Hence, such phenomena as flares resulting from tidal stripping of atmospheres of giant stars (MacLeod, Guillochon, & Ramirez-Ruiz 2012; Guillochon & Ramirez-Ruiz 2013) or stellar tidal disruption flares from recoiling SMBHs (Komossa 2012) are not considered due to the lack of observational data associated with them (see Alexander 2012 for a review of various dynamical channels by which stars can be supplied to a SMBH).

[2] Extended ROentgen Survey with An Imaging Telescope Array
[3] Astronomical Roentgen Telescope – X-ray Concentrator

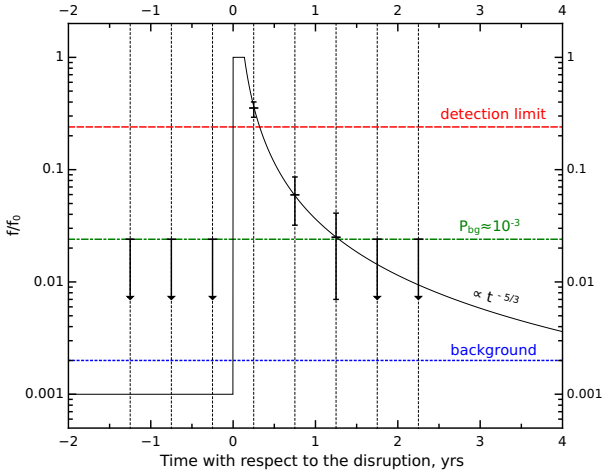

Figure 1. Light curve of a TDE candidate (normalized to the flux value at peak f_0) as would be seen by eROSITA. The source falls into the telescope's field of view every 6 months, as indicated by the vertical lines. The average background level is shown by the blue dotted line. The green dash-dotted line marks the count rate that can be produced by Poisson fluctuations in the background with a probability $P_{bg} \simeq 10^{-3}$. The flux from a TDE candidate must exceed this level by a factor $\geqslant$ 10 during at least one scan, which defines the TDE detection level shown by the red dashed line. See Appendix for further details.

2.1 Temporal properties

The flux decay of TDE flares is broadly consistent with a power law with a slope of $\sim -5/3$ (Komossa 2002; Halpern, Gezari, & Komossa 2004; Vaughan, Edelson, & Warwick 2004). This decay probably reflects the decreasing accretion rate, $\dot{M}$, of the falling back stellar material by the SMBH, coupled with some constant radiative efficiency ϵ (the source luminosity $L = \epsilon\dot{M}c^2$), since the viscous timescale is believed to be shorter than the characteristic dynamical fallback time (Rees 1988; Phinney 1989). However, Lodato et al. (2009) found that a $t^{-5/3}$ decrease of $\dot{M}$ is reached only asymptotically at late times, while at earlier stages the behavior of the accretion rate is sensitive to the structure of the disrupted star. Besides that, the radiative efficiency of accretion is probably constant only at a certain phase of the event, namely when $\dot{M}$ is below the critical value $\dot{M}_{Edd} = \epsilon^{-1}L_{Edd}/c^2$ corresponding to the Eddington luminosity $L_{Edd} \backsimeq 1.3{\times}10^{44}\left(\frac{M_{BH}}{10^6 M_\odot}\right)$ erg s^{-1}, but still above $\sim 0.01\dot{M}_{Edd}$. At this stage, the released gravitational energy is radiated away by a geometrically thin, optically thick accretion disk (Shakura & Sunyaev 1973). For a solar type star with a pericenter distance $R_p = 3R_S$ (where R_S is the Schwarzschild radius), the peak mass rate occurs at time

$$\tau_i \backsimeq 20\left(\frac{M_{BH}}{10^6 M_\odot}\right)^{5/2} \text{ min} \qquad (1)$$

after the instant of disruption t_0 and is highly supercritical given $\epsilon = 0.1$ and $M_{BH} \lesssim 10^7 M_\odot$ (Strubbe & Quataert 2009; this delay is in fact highly sensitive to pericenter distance: $\tau_i \propto R_p^3$). Therefore, early on accretion takes place in radiatively inefficient regime, with an approximately constant luminosity $L \backsimeq L_{Edd}$ emitted by a thick accretion disk, which is likely subject to outflows (Ulmer 1999; Strubbe & Quataert 2009). The boundary between the early (Eddington) and late (decay) phases lies at

$$\tau_{Edd} \backsimeq 0.1 \left(\frac{M_{BH}}{10^6 M_\odot} \right)^{2/5} \text{ yr} \quad (2)$$

after disruption for $R_p = 3R_S$ ($\tau_{Edd} \propto R_p^{6/5}$, Strubbe & Quataert 2009). Although the reality can be somewhat more complicated (see e.g. Lodato et al. 2009), we adopt the following approximate relation for the time profile of flares associated with TDEs:

$$L(t) = \begin{cases} L_{quies} & \text{for } t < t_0 \\ L_0 & \text{for } t_0 < t < t_1 \\ L_0 \left(\frac{t-t_0}{\tau_{Edd}} \right)^{-5/3} & \text{for } t > t_1 \end{cases} \quad (3)$$

where L_{quies} is the source luminosity in the quiescent state, $L_0 = \eta L_{Edd} \gg L_{quies}$ is the peak observed luminosity (with η being a geometrical dilution factor), and $t_1 = t_0 + \tau_{Edd}$. Equation (3) ignores the short period $\tau_i \ll \tau_{Edd}$ since $\tau_i/\tau_{Edd} \simeq 4 \times 10^{-4} \left(M_{BH}/10^6 M_\odot \right)^{21/10} \left(R_p/3R_S \right)^{9/5}$. However, as we further discuss in Section 4.2 below, there is an interesting possibility to observe some TDEs during the rising phase of the flare, which lasts $\tau_{rise} < \tau_i \ll \tau_{Edd}$ (under our assumption of shortness of the viscous time compared to the fallback time) and can be significantly long for large M_{BH} and/or R_p.

For SMBHs with $M_{BH} \gtrsim \text{few} \times 10^7 M_\odot$, only the closest stellar disruptions (small R_p) can lead to supercritical accretion, while the majority of TDE flares associated with such SMBHs are expected to be sub-Eddington (given a uniform distribution of pericenters, Ulmer 1999). Moreover, most of the emission will appear at UV rather than X-ray energies (see Section 2.2 below). We thus restrict our consideration to SMBHs with $M_{BH} \lesssim 10^7 M_\odot$.

We note that very recent analytic (Stone, Sari, & Loeb 2012) and numerical (Guillochon & Ramirez-Ruiz 2013) calculations indicate that the characteristic timescales discussed above might be almost independent of R_p, since the stellar debris energy 'freezes in' at the tidal radius $R_t = R_\star \left(M_{BH}/M_\star \right)^{1/3}$ (where $R_\star$ and $M_\star$ are the mass and radius of the disrupted star), rather than at R_p as was thought before (see Stone, Sari, & Loeb 2012 for a thorough discussion). The resulting difference is small for $M_{BH} = 10^7 M_\odot$ (since $R_t/3R_S = 1.6$, assuming $R_\star = R_\odot$ and $M_\star = M_\odot$), but becomes significant for lighter SMBHs, since $R_t/3R_S = 7.5$ for $M_{BH} \sim 10^6 M_\odot$, which should lead to longer τ_i and τ_{Edd} and hence to slower flux decay during the post-peak phase. However, there is no observational confirmation of these new theoretical results yet. Furthermore, the TDE light curves observed so far are consistent with the shorter decay time-scales expected for $R_p \sim 3R_S$ (Esquej et al. 2008). Since we make our predictions for the eROSITA TDE detection rate (in Section 4) using the same (currently available) data set, we shall for simplicity assume $R_p = 3R_S$.

2.2 Spectral properties

An observer will detect only a fraction of the TDE bolometric flux, depending on the spectral energy distribution of TDE emission and the energy response of the detector used. Since this emission presumably originates in an accretion disk around a SMBH, its spectral energy distribution can be approximated (Shakura & Sunyaev 1973) by a black body radiation spectrum with temperature

$$\kappa T_{bb} \simeq 0.06 \left(\frac{M_{BH}}{10^6 M_\odot} \right)^{-1/4} \left(\frac{\dot{M}}{\dot{M}_{Edd}} \right)^{1/4} \text{ keV}, \quad (4)$$

which corresponds to the innermost regions of the disk ($R \sim 5R_S$, Ulmer 1999). Since this emission is fairly soft, the detection probability must strongly depend on the absorption column density to the source, implying that X-ray selected samples might be biased against absorbed TDE events. No indication of significant intrinsic absorption has been found from spectral analysis performed for known TDE candidates under the assumption of black body emission. The estimated black body temperatures are $\kappa T_{bb} \simeq 0.07$ keV (the median value, Komossa 2002; Esquej et al. 2008), although the quality of the existing X-ray data hardly makes it possible to distinguish a black body model from e.g. an absorbed power-law model (Esquej et al. 2008). Power-law fits typically resulted in steep slopes ($\Gamma \gtrsim 3$), i.e. the observed spectra are indeed soft.

Disregarding the remaining uncertainty in the spectral shape of TDE emission, we use the (physically motivated) absorbed black body model in our calculations. This model has 3 parameters: absorption column density N_H, temperature κT_{bb} and peak bolometric flux

$$f_0 = \frac{L_0}{4\pi d_L^2}, \quad (5)$$

where d_L is the luminosity distance to the source (see Section 4). We freeze the first parameter at $N_H = 5 \times 10^{20}$ cm^{-2}, which is close to the median value of Galactic absorption for random positions in the extragalactic sky as calculated by Esquej et al. (2008). In addition to the Galactic absorption there might also be some intrinsic absorption due to edge-on orientation of the accretion disk and/or screening by unbound stellar debris material (Strubbe & Quataert 2009). However, in the former case the disk radiation might be directed preferentially away from the observer, and so the contribution of such events to the net detection rate is likely to be small. In the latter case, the estimates of Strubbe & Quataert (2009) indicate that unbound equatorial material builds up a 'vertical wall' of debris with huge column density in the radial direction but subtending a small solid angle $\Delta\Omega \sim 0.1$ sr. Such screening will most likely result in complete non-detection rather than detection of a TDE with a significant excess of absorption relative to the Galactic value.

As follows from Eq. 4, the second parameter of the model obeys $\kappa T_{bb} \propto M_{BH}^{-1/4}$. Unfortunately, there are only crude M_{BH} estimates for known TDE candidates. The median observed temperature $\kappa T_{bb} \simeq 0.07$ keV implies a SMBH with mass $M_{BH} \approx 10^6 M_\odot$. For comparison, for $M_{BH} = 5 \times 10^6$ and $10^7 M_\odot$ one expects $\kappa T_{bb} = 0.047$ and 0.039 keV, respectively. We shall use these three fiducial values in our calculations.

As the accretion rate of falling back material decreases, the effective temperature of the radiation is also expected to decrease as $\kappa T_{bb} \propto \dot{M}^{1/4}$, as long as the thin disk approximation remains valid (Strubbe & Quataert 2009). Nonetheless, late observations of five TDE candidates from RASS (Vaughan, Edelson, & Warwick 2004) demonstrated no significant softening and in fact indicated a marginal hardening for some of them, while the luminosities fell by more than two orders of magnitude[4]; Komossa et al. (2004) found similar spectral hardening for another TDE candidate, RX J1242–1119. This behavior may have resulted from transition to a different accretion mode accompanied by Comptonization of disk radiation in a hot corona and/or significant contribution from a relativistic jet. Taking into account these observations and because we expect eROSITA to detect TDEs mostly during an early post-peak phase (see Section 4), we disregard possible spectral evolution of TDE-associated emission in our estimates below.

It is also worth mentioning that somewhat higher temperatures ($\kappa T_{bb} \sim 0.12$ keV) have been reported for TDE can-

[4] It should be mentioned that the host galaxies of some of these candidates are classified as hosting an active nucleus.

didates detected in clusters of galaxies (Cappelluti et al. 2009; Maksym, Ulmer, & Eracleous 2010). It is unclear whether this is owing to some selection bias, the specific physical environment and/or details of the spectral analysis. In any case, searches for TDE candidates with eROSITA in galaxy clusters will be challenging due to the strong diffuse X-ray emission from the hot intracluster gas (which is much less of an issue for *Chandra*, Maksym, Ulmer, & Eracleous 2010), except for brightest flares in nearby clusters (like the one reported by Cappelluti et al. 2009), for which elaborate spectral analyses can be performed taking advantage of eROSITA's higher sensitivity below 0.3 keV compared to *Chandra*. A further advantage in studying such events might be that galaxy clusters belong to the main scientific targets of eRASS (Merloni et al. 2012) and will thus be extensively covered by follow-up observations.

3 OBSERVATIONAL TECHNIQUE

In formulating TDE identification criteria we should address the *completeness* of the resulting sample and *reliability* of the selection procedure. As usual in such cases (see e.g. Chapter 7 of Wall et al. 2003), if we wish to maximize the number of sources of the required type, we should be ready to deal with significant contamination of the sample by misidentified sources. In the case of eRASS, our primary goal is to obtain as large as possible a sample of TDE candidates that will make it possible to accurately measure the rate of such events in the local Universe. The associated systematic bias could then possibly be corrected by weighting the candidates according to their reliability. Hence, we choose rather loose identification criteria, based on key signatures of TDEs.

3.1 eROSITA All-Sky Survey

The *SRG* satellite will be rotating with a period of $T = 4$ hours around its axis pointed within a few degrees of the Sun, with the telescopes observing the sky at right angles to the axis (Merloni et al. 2012). Following the orbit of the L2 point around the Sun the rotation axis will be moving at a speed of 1 deg per day. With the 1 deg-diameter field of view (FoV), eROSITA will complete an all-sky survey every 6 months and a total of 8 scans will be performed over the course of the mission. A typical position on the sky will receive $\sim$ 240 seconds of exposure during one scan. This exposure will be achieved by 6 consecutive passages of a source through the eROSITA FoV separated by $\sim$ 4-hour intervals (see Khabibullin, Sazonov, & Sunyaev 2012 for further details). A typical visit of a point source will thus last $\sim$ 1 day, which is much shorter than the expected characteristic timescale of the flux decay during a TDE flare (few months). Hence, we shall regard such visits as single 240 s-long observations.

We note that in reality the eRASS exposure is not constant over the sky and increases with ecliptic latitude. Most importantly, there are two areas of $\sim$ 1000 deg^2 each, surrounding the ecliptic poles, that will be visited more than 20 times during each eROSITA all-sky scan (Merloni et al. 2012). Hence, the threshold for detecting TDE flares in these regions will be $\sim$ 4 times lower than the all-sky average used in our analysis below. That will not only allow one to detect weaker TDE flares (including events from more distant galaxies) but also to study in greater detail the X-ray light curves of bright TDE flares. This can be particularly important for detecting TDEs during their rise phase (See Section 4.2).

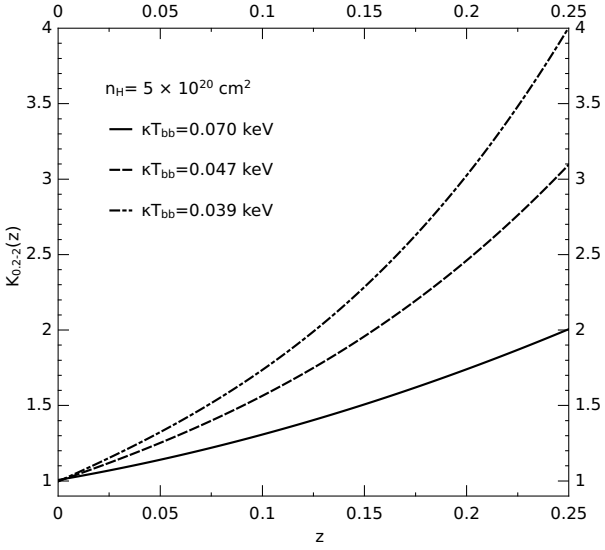

Figure 2. Redshift spectral correction $K_{0.2-2}(z)$ for various spectral models representing spectra of TDE flares from SMBHs with $M_{BH} = 10^6 M_\odot$ (black body with $\kappa T_{bb} \simeq 0.070$ keV), $M_{BH} = 5 \times 10^6 M_\odot$ (black body with $\kappa T_{bb} \simeq 0.047$ keV), $M_{BH} = 10^7 M_\odot$ (black body with $\kappa T_{bb} \simeq 0.039$ keV). All spectra were modified by Galactic absorption with $N_H = 5 \times 10^{20}$ cm^2.

3.2 Identification criteria

For a TDE with a given spectral energy distribution, bolometric flux f (see Subsection 2.2) and redshift z, the count rate measured by eROSITA between 0.2 and 2 keV can be written as

$$C_{0.2-2}(f,z) = \frac{A_{0.2-2}}{K_{0.2-2}(z)} f, \quad (6)$$

where $A_{0.2-2}$ (in units of counts cm^2/erg) is the flux-to-count conversion factor for a TDE at $z \to 0$ and the correcting factor $K_{0.2-2}(z)$ accounts for the cosmological reddening of the spectrum. Both $A_{0.2-2}$ and $K_{0.2-2}$ depend on the eROSITA response matrix and TDE spectrum. We have computed the redshift correction for different relevant spectral models using XSPEC (Dorman & Arnaud 2001), and it proves to be significant (see Fig. 2), especially for the model corresponding to $M_{BH} = 10^7 M_\odot$. This has an obvious explanation: as the intrinsic TDE spectrum becomes softer with increasing black hole mass, a largely fraction of the photons red-shift out of the eROSITA energy band into softer bands (below 0.2 keV).

Disregarding spectral evolution during the TDE, the count rate varies with time as $C_{0.2-2}(t_{observer}) \propto L\,(t_{source}(t_{observer}))$, where the relation $t_{source}(t_{observer})$ is governed by the source's redshift.

Additional information on the nature of TDE candidates can be obtained by dividing the 0.2–2 keV energy band into several subbands, e.g. 0.2–0.4, 0.4–1 and 1–2 keV. The first one is sensitive to absorption along the line of sight, whereas the other two are well suited for estimating the effective spectral slope. We thus introduce a softness ratio $SR = C_{0.4-1}/C_{1-2}$ to distinguish 'soft' and 'hard' sources (see Appendix for further details).

Taking into account the anticipated TDE properties (see Section 2) and eRASS characteristics (see Section 3.1), we propose to discriminate TDEs against other types of X-ray transients to be detected during the survey (such as AGN flares and GRB afterglows, see e.g. Komossa 2002) based on the following two signatures:

- large ($\geqslant$ 10) variation between the count rates ($C_{0.2-2}$) measured in two consequent half-a-year scans (see Fig. 1);

• soft spectrum (as indicated by the softness ratio SR), consistent with a weakly absorbed ($N_H < 10^{21}$ cm^{-2}) power law with a photon index $\Gamma \geqslant 3$.

In addition, since we are dealing with soft X-ray flares, it is reasonable to limit TDE searches to Galactic latitudes $|b| > 30°$, where interstellar absorption $N_H < 10^{21}$ cm^{-2}. That will also minimize contamination from cataclysmic variables and flaring dM stars, whose appearance can resemble TDEs (see Donley et al. 2002).

Although the peak X-ray flux during a TDE can greatly exceed the corresponding quiescent flux, i.e. the flux produced by the TDE's host galaxy, in reality the minimum flux will, in most cases, be dominated by the eROSITA background (see Appendix). Therefore, the first of our requirements formulated above implies that a candidate TDE must be at least 10 times as bright as the background. Besides that, the count rate must be high enough for the softness ratio SR to indicate that $\Gamma > 3$ rather than $\Gamma \sim 2$ as typical of AGN. As demonstrated in Appendix, these conditions imply that at least $N_{lim} = 40$ counts (i.e. 20 counts inside the half power diameter region) must be collected from a source between 0.2 and 2 keV during a 240 s exposure. The corresponding bolometric flux limits f_{lim} for various spectral models are given in Table 1. Figure 3 shows a simulated eROSITA spectrum (for $M_{BH} = 10^6 M_\odot$) of a TDE with $f = f_{lim}$. Trial fits of this spectrum by various characteristic models demonstrate that it is feasible to reveal the spectral softness of a TDE using ~ 40 counts.

We can finally formulate exact criteria that can be used for identification of TDE candidates during eRASS:

1. Extragalactic ($|b| > 30°$) location.
2. At least 40 counts (or 20 counts inside the half power diameter region) detected from the source during the ~ 240 s exposure in a given scan of the sky.
3. At least a factor of 10 higher count rate in comparison with the preceding or succeeding scan.
4. Softness ratio $SR \geqslant 2$ in the bright state.

The last criterion should not be used in application to relativistic TDEs, a subclass of TDEs discussed in Section 4.4 below.

3.3 Detection in subsequent eRASS scans

A TDE X-ray flare discovered in a given eRASS scan can remain detectable by eROSITA in its subsequent sky scans, i.e. 6 months, 12 months etc. after the TDE trigger. This provides an interesting possibility of obtaining a crude (2 or more data points) long-term light curve of TDE emission. Specifically, to obtain a significant (see Appendix for details) X-ray detection from a continuing TDE flare (whose position is known from its initial observation by eROSITA), just ~ 4 counts during the ~ 240 s exposure are required. This implies, for instance, that a TDE flare will be detectable by eROSITA even if the X-ray flux has dropped by an order of magnitude during 6 months after the trigger. Such late detections, or even upper limits provided by non-detections, will be very useful for testing TDE models.

4 PREDICTIONS

The intrinsic rate, $\mathcal{R}$, of tidal disruption events in the local Universe, i.e. the number of TDEs per unit time and unit volume,

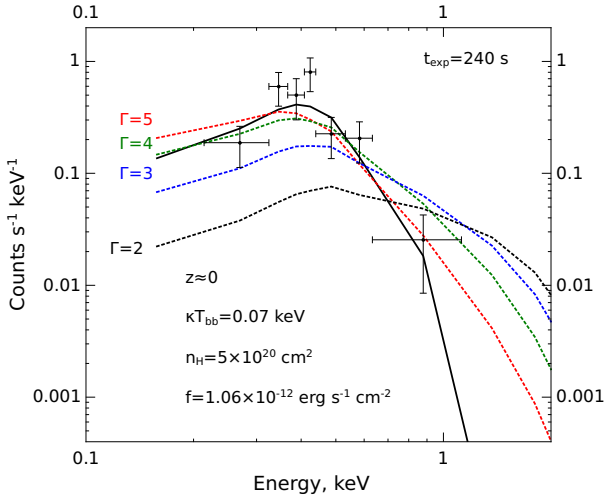

Figure 3. Simulated eROSITA spectrum of a TDE at $z \approx 0$ with flux near the eRASS detection threshold, i.e. providing 40 counts during 240 s exposure time. The adopted TDE spectral model corresponds to $M_{BH} = 10^6 M_\odot$ (see text) and the corresponding bolometric flux is 1.06×10^{-12} erg s^{-1} cm^{-2}. The spectrum is binned in energy so that the significance of data points is 2σ. Also shown are best fits of the data by different models: solid – absorbed blackbody emission, dashed – absorbed power laws ($N_H = 5 \times 10^{20}$ cm^{-2}) with the indicated slopes. In this example, an absorbed power law with $\Gamma \leqslant 3$ can be rejected with ≈99% significance based on χ^2 statistics with the weighting suggested by Churazov et al. 1996 for spectral analysis in the case of low number of counts.

should depend on a number of factors, such as the mass distribution of SMBHs and the density profiles of nuclear stellar cusps, which are fairly uncertain at present. Hence, it is difficult to predict the TDE discovery rate for eRASS based on theoretical grounds. However, we can try to estimate this rate using the existing (poor) statistics of TDEs. Specifically, we can make use of an estimate based on the detection of two candidates in the *XMM-Newton* Slew Survey and their non-detection in RASS: $\mathcal{R} \simeq 5 \times 10^{-6}$ yr^{-1} Mpc^{-3} (Esquej et al. 2008). Despite having a rather high uncertainty and probably being affected by selection effects (see Gezari et al. 2009), this estimate is in line with other observational results (Maksym, Ulmer, & Eracleous 2010) and with some theoretical expectations (Wang & Merritt 2004).

4.1 Detection rate

We assume ΛCDM cosmology with $\Omega_M = 0.275, \Omega_\Lambda = 0.725$ and $h = 0.7$ (Komatsu et al. 2011). The luminosity distance as a function of redshift is then given by

$$d_L(z) = (1+z)\, d_H \int_0^z \frac{dz'}{E(z')}, \tag{7}$$

where $d_H = \frac{c}{H_0} \approx 3.0 h^{-1}$ Gpc ≈ 4.3 Gpc is the Hubble distance, and $E(z) = \sqrt{\Omega_m (1+z)^3 + \Omega_\Lambda}$ (Hogg 1999). Defining $J(z) = \int_0^z \frac{dz'}{E(z')}$, equation (7) becomes $d_L(z) = d_H (1+z) J(z)$.

Given the flux detection limit f_{lim} corresponding to a given spectral model (Table 1), there exists the largest distance $d_{L,lim}$ (or the corresponding redshift z_{lim}) from which a TDE flare at its peak could be identified with eROSITA:

$$\frac{L_0}{4\pi d_L(z_{lim})^2 K(z_{lim})} = f_{lim} \tag{8}$$

Table 1. Summary of the results. The adopted TDE intrinsic rate $\mathcal{R}$ is a crude estimate based on the currently available sample of X-ray selected TDEs (see text). It is assumed that all TDEs are associated with SMBHs of the same mass M_{BH}, for which three fiducial values are used. The detection limit is given in terms of the black body spectrum normalization $f = L_b/(4\pi d_L^2)$, where L_b is the bolometric luminosity and d_L is the luminosity distance to the source. The quantity $\mathcal{N}$ gives the total number of TDEs with the 0.2–2 keV flux above the appropriate detection limit. It is not corrected for those events that were already detected in the preceding scans (see the next column for the relative fraction of such events). The next two columns provide the relative fractions of events that are triggered in the supercritical and rising phases of their light curves. The relative fraction of events for which eROSITA will provide at least 2(or 3) significant data points for constructing a long-term ($\geqslant$ 6 months) X-ray light curve (see Section 3.3) is given in the last column.

Model	κT_{bb} (keV)	$\mathcal{R}$ / 10^{-5} (yr/ Mpc^3)	f_{lim} / 10^{-12} (erg/ s/ cm^2)	z_{lim}	$\mathcal{N}$ per scan	Fraction of events in $\geqslant 2$ scans	in Edd. phase	in rising phase	with $\geqslant$ 2(3)-point light curve
$M_{BH} = 10^6 M_\odot$	0.070	0.5	1.06	0.164	650	$\sim 1/12$	$\sim 1/2$	$\lesssim 4\times10^{-4}$	$\sim 4/5$ (7/20)
$M_{BH} = 5\times10^6 M_\odot$	0.047	0.5	4.29	0.162	1240	$\sim 1/4$	$\sim 1/2$	$\lesssim 1\times10^{-2}$	~ 1 (16/20)
$M_{BH} = 10^7 M_\odot$	0.039	0.5	10.81	0.142	1150	$\sim 1/3$	$\sim 1/2$	$\lesssim 5\times10^{-2}$	~ 1 (19/20)

or

$$(1+z_{lim})^2\, J\,(z_{lim})^2\, K\,(z_{lim}) = \frac{L_0}{4\pi d_H^2 f_{lim}}. \quad (9)$$

Solving this equation numerically with $L_0 = 1.3\times10^{44}$ erg s^{-1} (the Eddington luminosity for a black hole with mass $M_{BH} = 10^6 M_\odot$ and geometrical dilution factor $\eta = 1$), we obtain $z_{lim} = 0.164$. This is approximately two times further than the distance within which TDEs could be found with RASS ($z \approx 0.09$, Donley et al. 2002; Esquej et al. 2008). Similar calculations for $M_{BH} = 5\times10^6$ and $10^7 M_\odot$, again assuming the Eddington luminosity at the peak phase, result in $z_{lim} = 0.162$ and 0.142, respectively. Remarkably, the limiting redshifts for the different SMBH masses prove to be similar. This happens because although the peak TDE bolometric luminosity increases with M_{BH}, the spectrum becomes softer and most of the emission appears at frequencies below the eROSITA energy range.

Consider now a small volume of the Universe at redshift z with radial width dz, covering an opening angle ω on the observer's sky. The comoving volume of the slice is

$$dV_c\,(z) = \omega d_H^3 \frac{J\,(z)^2}{E\,(z)} dz \quad (10)$$

(Hogg 1999; see also Chapter 13 of Peebles 1993). Neglecting any evolutionary changes in the galaxy population between z_{lim} and $z = 0$, we can calculate the rate of TDEs in this volume as $d\mathcal{N}\,(z) = \mathcal{R} dV_c\,(z)\, dt$.

Taking into account both the maximum and decay phases of the light curve (eq. (3)), a TDE flare remains detectable during a comoving time

$$\tau_{lim}\,(z) = \tau_{Edd}\left(\frac{L_0}{4\pi d_H^2 f_{lim}} \frac{1}{(1+z)^2\, J\,(z)^2\, K\,(z)}\right)^{3/5}. \quad (11)$$

Hence, at a given moment of observation there are

$$d\mathcal{N}\,(z) = \mathcal{R} \times \tau_{lim}\,(z) \times dV_c\,(z) \quad (12)$$

detectable TDEs. Substituting the corresponding expressions for $dV_c\,(z)$ and $\tau_{lim}\,(z)$ and integrating from $z = 0$ to z_{lim}, we obtain the total number of detectable TDEs:

$$\mathcal{N} = \alpha \times I(z_{lim}), \quad (13)$$

where

$$\alpha = \omega \mathcal{R} d_H^3 \tau_{Edd} \left(\frac{L_0}{4\pi d_H^2 f_{lim}}\right)^{3/5} \quad (14)$$

and

$$I(z_{lim}) = \int_0^{z_{lim}} \frac{K\,(z)^{-3/5}\, J\,(z)^{4/5}}{(1+z)^{6/5}\; E\,(z)} dz. \quad (15)$$

Finally, expressed in convenient units, the total number of detectable TDEs at a given moment is

$$\mathcal{N} \simeq 9.51\times10^4 \left(\frac{\omega}{2\pi}\right)\left(\frac{\mathcal{R}}{10^{-5}}\right)\left(\frac{\tau_{Edd}}{0.1}\right)\left(\frac{L_0}{10^{44}}\right)^{3/5}\left(\frac{f_{lim}}{10^{-12}}\right)^{-3/5} I\,(z_{lim})\,. \quad (16)$$

4.2 Dependence on M_{BH} and the phase of the TDE light curve

Estimates of the SMBH mass function (Hopkins, Richards, & Hernquist 2007; Greene & Ho 2007) indicate that the spatial density of SMBHs is roughly constant in the mass range from $\sim 10^6$ to $10^7 M_\odot$ but depends on redshift. The TDE rate may demonstrate some correlation (Brockamp, Baumgardt, & Kroupa 2011) or anti-correlation (Wang & Merritt 2004) with the central SMBH mass. Therefore, since the maximum TDE distance for eRASS is almost independent of SMBH mass, we may expect the TDEs found during eRASS to be distributed over the M_{BH} range from $\sim 10^6$ to $\sim 10^7 M_\odot$. Since this distribution is currently unknown, we consider three different scenarios in which all TDEs detected during eRASS are characterized by a fixed M_{BH} value: 10^6, 5×10^6 or $10^7 M_\odot$. The resulting estimates are summarized in Table 1.

For $M_{BH} = 10^6 M_\odot$ and adopting $\mathcal{R} = 5\times10^{-6}$ yr^{-1} Mpc^{-3}, $\omega = 2\pi$ (which corresponds to the $|b| > 30^\circ$ sky) and $R_p = 3R_S$, we find from equations (2) and (15) that $\tau_{Edd} = 0.1$ yr and $I\,(z_{lim}) \approx \frac{1}{4.5} z_{lim}^{1.5} = 0.0153$, and finally from equation (16) that $\mathcal{N} \approx 650$ events can be discovered in the second eRASS scan through comparison with the first one. Figure 4 shows the distribution of the TDE flares over redshift and as a function of time passed after stellar destruction. Approximately half of the TDE triggers are expected to take place during the supercritical accretion phase. For $\sim 1/12$ of the events, a second trigger (during the subsequent eRASS scan) will be possible, and in rare cases, three or more independent triggers will be possible. Thus, the majority of TDEs will be 'new' for each scan, i.e. not seen during the preceding one. For $M_{BH} = 5\times10^6$ and $10^7 M_\odot$, the fraction of 'old' TDEs, i.e. events observed in more than one eRASS scan is higher (Fig. 5 and Fig. 6) since the characteristic decay time positively correlates with the black hole mass (see Section 2).

Besides that, it turns out that the majority of TDEs discovered in a given eRASS scan will still be detectable (i.e. significantly exceeding the background flux level) by eROSITA (see Section 3.3) in the subsequent sky scan(s), i.e. 6 months, 12 months etc. after

the initial trigger. Hence, eROSITA will typically provide 2–4 significant data points for constructing a long-term X-ray light curve of a TDE flare (see Table 1 and Figs. 4–6). As a result, eRASS will provide a unique sample of TDE light curves, which can be used to test TDE models.

The above estimates were based on the assumption that the peak accretion rate exceeds the Eddington limit. In reality, only TDEs caused by sufficiently close stellar passages can provide a supercritical accretion rate, whereas more distant disruptions may be characterized by subcritical maximum accretion rates. Since the Eddington limit increases proportionally to the SMBH mass, the fraction of sub-Eddington TDEs may become significant for high M_{BH}; e.g. Ulmer (1999) estimate that the peak accretion rate exceeds the Eddington limit in approximately 100% of events for $M_{BH} \sim 10^6 M_\odot$ and in $\sim 50\%$ for $M_{BH} = 10^7 M_\odot$. In such a case, our estimates for the number of TDEs detected during eRASS should be reduced accordingly.

As was mentioned in Section 2.1, there is a non-negligible chance of detecting some TDEs during the rising phase of the X-ray flare, especially for large M_{BH} and/or R_p. We may place a rough upper limit on the number of such triggers: $\mathcal{N}_{rise}/\mathcal{N}_{Edd} \lesssim \tau_i/\tau_{Edd}$, where $\mathcal{N}_{Edd}$ is the number of TDEs detected during the supercritical phase. For $M_{BH} = 10^7 M_\odot$, up to ~ 20 rising TDE flares can appear in each eRASS scan (see Table 1). Since the rising phase is expected to last between a fraction of an hour and a few days, it might in fact be possible to see how the X-ray transient brightens up between its $\gtrsim 6$ consecutive passages through the eROSITA FoV every ~ 4 hours.

As we noted before, there are two regions in the sky that will receive significantly increased exposure during eRASS, with more than 20 consecutive passages of a given source through the eROSITA's FOV. These regions are centered around the Northern and Southern ecliptic poles (NEP and SEP), with $b \simeq 30^\circ$ and $b \simeq -30^\circ$, respectively, and so, unfortunately, about half of the area of these 'deep fields' proves to be outside our proposed $|b| > 30^\circ$ TDE search region. Furthemore, the 'extragalactic', i.e. $|b| > 30^\circ$, part of the SEP region contains the Large Magellanic Cloud, which will probably also complicate detection of TDE flares there. As regards the NEP region, TDE flares of given luminosity could be detected from ~ 1.5 times larger distances (z_{lim}) than elsewhere, as a result of the 4-fold increase in sensitivity (see Eq. 9). Therefore, according to Equations (14, 16), one might expect a ~ 4 times higher TDE rate (per unit solid angle) in the NEP region compared to the average over the sky.

4.3 Revealing TDEs through eRASS–RASS comparison

Apart from comparing the results of successive eRASS sky scans, TDEs can also be discovered by cross-correlating the data of the first eRASS scan with RASS data[5]. The characteristic unabsorbed 0.5–2 keV flux limit for RASS point sources is 3×10^{-13} erg s^{-1} cm^{-2} (Brandt & Hasinger 2005). Hence, to detect a factor of 10 increase in flux, a candidate TDE must reach a 0.5–2 keV flux $> 3 \times 10^{-12}$ erg s^{-1} cm^{-2} during the first eRASS scan. This unabsorbed flux corresponds to a bolometric flux $f_{lim} \simeq 4.6 \times 10^{-12}$ erg s^{-1} cm^{-2} for the spectral model corresponding to $M_{BH} = 10^6 M_\odot$). This limit is approximately 4 times higher than for TDE detection based on eRASS scan-to-scan comparison (see Table 1). Solving equation (9) for f_{lim} results in $z_{lim} \simeq 0.095$. Using equation (16), we find that cross-correlation of the first eRASS

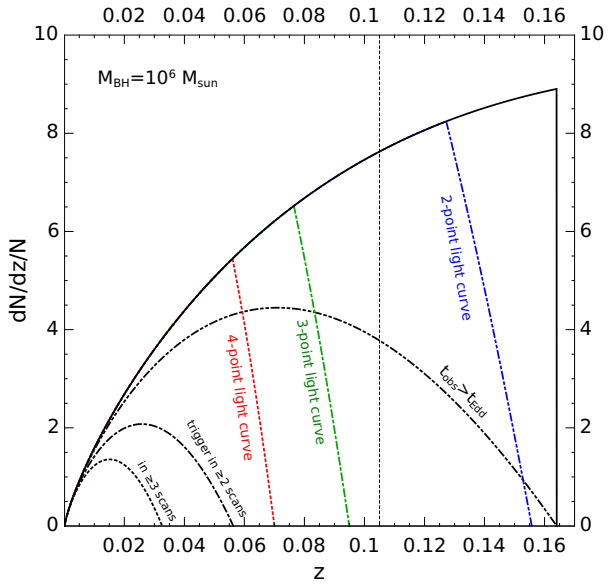

Figure 4. Distribution of TDE candidates over redshift for $M_{BH} = 10^6 M_\odot$. The total sample is shown by the solid black line. The events triggered as TDE candidates during the declining (post-supercritical) phase of the X-ray flare are shown by the two-dot-dashed black line. The events independently triggered as TDE candidates in more than one (two) eRASS scans are shown by the dot-dashed (dotted) black line. The blue, green and red lines denote events for which at least 2-,3- and 4-point X-ray light curve can be obtained using data from consecutive eRASS scans. The thin vertical dashed line marks the redshift at which the numbers of events triggered during the supercritical and declining phases are equal.

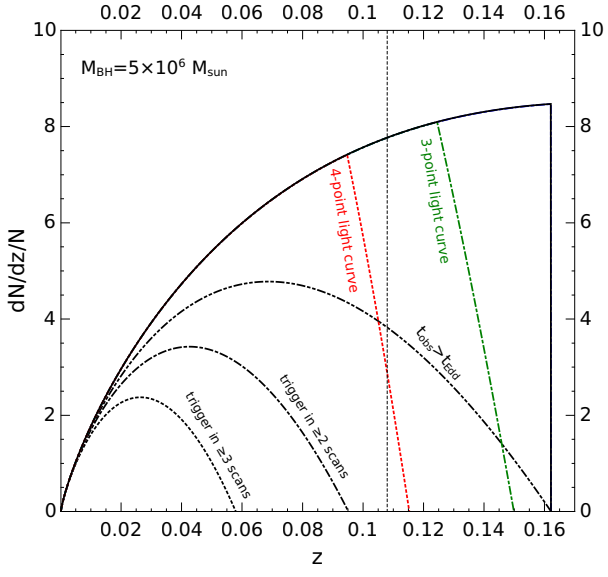

Figure 5. Same as Fig. 4 but for $M_{BH} = 5 \times 10^6 M_\odot$.

[5] The sky coverage of *Chandra* and *XMM-Newton* serendipitous surveys are too small for this purpose (see Brandt & Hasinger 2005), while the *XMM-Newton* Slew Survey is similar in sensitivity to RASS (below 2 keV) but effectively covers only about a third of the sky (Esquej et al. 2008)(see also Warwick, Saxton, & Read (2012) for a more recent reference).

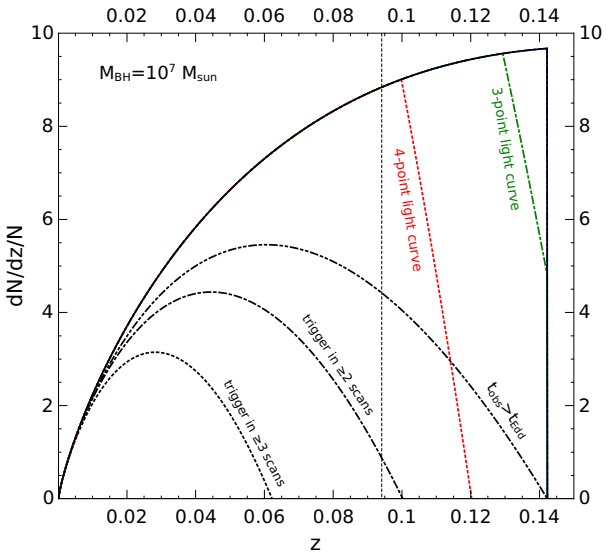

Figure 6. Same as Fig. 4 but for $M_{BH} = 10^7 M_\odot$.

scan with RASS will provide an additional $\sim$ 125 TDE candidates (assuming $\mathcal{R} = 5 \times 10^{-6}$ yr^{-1} Mpc^{-3}, $\omega = 2\pi$ and $M_{BH} = 10^6 M_\odot$.

In addition, $\sim$ 15 TDE candidates could be found using the method of Donley et al. (2002), i.e. by looking for *ROSAT* sources with soft X-ray spectra that were at least $\gtrsim$ 10 times brighter during RASS than in subsequent observations. In their study (Donley et al. 2002) used *ROSAT* PSPC data, which cover only $\sim$ 9% of the sky, for the follow-up, whereas with eRASS the analysis can be done for 50% of the sky ($|b| \geqslant 30^\circ$). Follow-up radio observations of such candidates could be useful for constraining models of TDE-associated jets (Bower et al. (2012); see Subsection 5.2).

4.4 Tidal disruption events with jets

Only two TDE flares with signatures of a relativistic jet have been discovered so far (Cenko et al. 2012). Moreover, these detections were triggered in the hard X-ray (15-50 keV) band by the Burst Alert Telescope (BAT) on *Swift*. Therefore, it is difficult to predict how many such transients can be found during eRASS.

A very rough estimate can be obtained by assuming that all TDEs with jets are similar to Sw J2058+05, the brightest *Swift* event of this type. Its estimated isotropic X-ray (0.3–10 keV) luminosity is $L_{X,iso} = 3 \times 10^{47}$ erg s^{-1} and the spectrum is consistent with a power law with $\Gamma \simeq 1.6$ absorbed by a column density $N_H \simeq 2.6 \times 10^{21}$ cm^{-2}, intrinsic to the source located at $z = 1.185$ (Cenko et al. 2012). We simulated an eROSITA observation of a source with such a spectrum at $z = 1$ and found that our count rate detection limit corresponds to an unabsorbed flux $F_{0.3-10} = 2.3 \times 10^{-12}$ erg s^{-1} cm^{-2} (we disregarded the K-correction since the spectral shape above 10 keV is unclear, whereas the spectrum below 10 keV is variable and corresponds to $K \simeq const$ for $z \gtrsim 1$). Assuming a peak isotropic X-ray (0.3–10 keV) luminosity[6] $L_{X,iso} \sim 5 \times 10^{47}$ erg s^{-1}, the limiting redshift is $z_{lim} \simeq 4.5$. Therefore, TDEs with jets can potentially be found with eRASS even in the distant Universe. Clearly, the actual number of such events will strongly depend on the cosmic evolution of galaxies and their nuclei. Ignoring the redshift dependence, the existing *Swift* statistics implies that roughly $\sim$ 1 TDE with jets may be detected during each eRASS scan.

An independent upper limit on the rate of TDEs with jets is provided by *ROSAT* data. The analysis of Donley et al. (2002) revealed only one high-amplitude ($\geqslant$ 20) flare with a hard spectrum ($\Gamma < 2$). This event is associated with the Seyfert 2 galaxy SBS 1620+545 (Carrasco et al. 1998) at $z = 0.0516$. On the *WISE* IR color–color diagram (Wright et al. 2010), the object falls on the boundary between Seyferts and spiral galaxies ([W1-W2]=0.6, [W3-W2]=2.9, Data Tag: ADS/IRSA.Gator#2012/1017/032431_5650). The observed-frame absorption-corrected 0.2–2.4 keV luminosity is $\sim 10^{43}$ erg s^{-1} in the bright state (Donley et al. 2002), which is much less than the observed luminosity of relativistic TDEs. Therefore, it seems more likely that this hard flare is an example of extreme variability in Seyfert 2 galaxies. Observation of SBS 1620+545 during eRASS will probably clarify the situation, since there have been no post-*ROSAT* X-ray observations of the source. Given that the same analysis of RASS data (Donley et al. 2002) revealed 5 soft flares – TDE candidates, we can tentatively conclude that the rate of relativistic TDEs is at least 5 times less than for 'ordinary' TDEs. Hence, perhaps not more than $\sim$ 150 relativistic TDEs will be detected during each eRASS scan.

In order to search for relativistic TDEs in eRASS data, one could use the same count rate criteria as for 'normal' TDEs (see Section 3.2) but the spectral softness criterion should obviously be omitted or modified so that it selects hard rather than soft X-ray flares.

5 DISCUSSION

In order to reveal the true nature of the numerous TDE candidates to be found during eRASS, some additional identification/follow-up work should be done, as we discuss below.

5.1 Cross-correlation with other surveys

The localization accuracy for point sources detected during eRASS is determined by the eROSITA point spread function (PSF) averaged over its FoV ($\simeq \varnothing 1^\circ$). For the faintest sources, it is expected to be $\sigma \simeq 12''$ (corresponding to a half-power diameter, HPD, of $\simeq 29''$, Merloni et al. 2012). Localization of bright sources, such as TDE candidates, can be significantly better since the centroid determination error is inversely proportional to the square root of the number of counts detected. Further improvement for TDE flares could be achieved using the fact that several of the total $\gtrsim$ 40 counts will be detected in the on-axis region of the telescope's FoV, where the HPD is $\sim 15''$ (Merloni et al. 2012). We may thus conservatively estimate that eROSITA should be able to localize TDE flares to better than 10". At redshifts typical of the eRASS TDE sample, $z \simeq 0.1$, the corresponding linear size is thus < 20 kpc. Such accuracy should be sufficient for searching for TDE host galaxies in optical (e.g. SDSS[7], SDSS-III Collaboration et al. 2012,

[6] This adopted value is somewhat higher than the luminosity measured for Sw J2058+05, but the corresponding *Swift*/XRT observations started some 10 days after the beginning of the hard X-ray flare and so may have missed the brightest phase of the event.

[7] http://www.sdss3.org/

and Pan-STARRS[8], Kaiser et al. 2010) and infrared (e.g. *WISE*[9], Wright et al. 2010) catalogs. However, association of a TDE candidate with the nuclear region of a galaxy will be possible only for bright flares and/or nearby galaxies.

Should the redshift of the likely host galaxy of a TDE candidate be known, it may immediately indicate a very high luminosity of the transient and hence exclude its extranuclear origin (i.e. a highly variable ultraluminous X-ray source). To additionally exclude soft X-ray flares from active galactic nuclei, an optical spectrum (Veilleux & Osterbrock 1987) and IR colors (Wright et al. 2010) of the counterpart galaxy could be used, if available[10]. Therefore, cross-correlation efforts can greatly help in confirming/rejecting the TDE nature of candidates found during eRASS.

5.2 Follow-up observations

The expected rate of 'TDE triggers' (see Section 4) during eRASS implies that there will be roughly two TDE alarms every day (data transfer from the spacecraft is planned to occur once a day). For some (perhaps a minority) of them, host galaxy identification will not be immediately clear. Optical follow-up observations for such events could clarify the situation and possibly also detect an optical signal associated with the TDE itself if carried out early enough after the TDE peak. Given the spectral energy distribution of TDE flares, it is more likely, however, to detect fading emission in X-ray (e.g. with *Chandra* or *XMM-Newton*) and/or UV (*GALEX*[11]) follow-up observations. Moreover, *Chandra* can provide excellent localization ($\lesssim 1''$) and a high quality spectrum in the 0.3–7.0 keV energy band after a few kilosecond observation (see, e.g., Vaughan, Edelson, & Warwick 2004). An even higher signal-to-noise spectrum can be provided by *XMM-Newton*. A complementary UV detection by *GALEX* would help constrain TDE emission models even better than with X-ray data alone (Gezari et al. 2009).

In addition, radio follow-up observations may be crucial for identification of relativistic TDEs, as has been the case for both events discovered by *Swift* (Metzger, Giannios, & Mimica 2012; Giannios & Metzger 2011; van Velzen, Körding, & Falcke 2011). On the contrary, searches for radio emission accompanying 'ordinary' TDEs have not yet given conclusive results (Bower et al. 2012; van Velzen et al. 2012).

We further note in this connection that blazar flares could in principle resemble relativistic TDEs. Indeed, blazar emission is also believed to originate in the vicinity of a SMBH from a relativistic outflow directed at the observer. However, the two relativistic TDEs discovered by *Swift* were clearly different from known blazar flares and from any other known types of transients in that i) the X-ray luminosity was very high and ii) the broad-band spectral energy distributions (from radio to hard X-ray) were inconsistent with the so-called blazar sequence, in particular the optical to X-ray luminosity ratio was very low (see Figs. 4–6 in Cenko et al. 2012). Therefore, follow-up observations will likely be able to discriminate relativistic TDEs from blazar flares among hard X-ray flares detected by eROSITA. We also note that identification of new blazars in eRASS data is an important scientific task by itself, which can be addressed by different known methods, e.g. using infrared colors provided by the *WISE* all-sky survey (Massaro et al. 2011).

6 CONCLUSIONS

We have demonstrated that eRASS will be very effective at finding stellar tidal disruption events. A uniquely large sample of several thousand TDE candidates can be obtained, making it possible to accurately measure the rate of stellar disruptions by SMBHs with masses from $\sim 10^6$ to $\sim 10^7 M_\odot$ and thus to obtain a census of dormant SMBHs and their associated nuclear stellar cusps in the local Universe (within $z \sim 0.15$). Roughly half of the TDEs will be observed by eROSITA during the supercritical (Eddington) phase of accretion and the rest during the subsequent decay. In addition, there might be up to $\sim 10^2$ TDE flares caught during the rising phase, i.e. when the debris of the disrupted star have just reached the black hole. Furthermore, for the majority of the TDE candidates, eROSITA will still be detecting their fading X-ray emission in 1–3 subsequent sky scans, i.e. 6–18 months after the initial trigger. Hence, a unique sample of TDE light curves will be obtained, diminishing the need for dedicated X-ray follow-up efforts. There will thus be plenty of information on various stages of accretion of stellar material by SMBHs, setting stringent constraints on TDE theory.

Importantly, TDE candidates can be recognized as such almost immediately (within a day) after their detection by eROSITA, so that prompt multiwavelength follow-up observations can be organized. Such dedicated efforts may lead to the discovery of peculiar events among the many TDEs discovered by eRASS, e.g. associated with a rapidly rotating SMBH or with the disruption of a rare type of star or a planet (such as the recently discovered hard X-ray transient IGR J12580+0134, Nikolajuk & Walter 2013).

Of particular interest is the possibility of obtaining a substantial sample of relativistic TDEs. Due to their extreme power, such transients can be detected by eRASS up to great distances ($z \sim 4$). The increased sample can shed light on the relation of jet-dominated TDE flares to 'normal' ones. Detection of relativistic TDEs at large redshifts will also provide a unique opportunity to study quiescent SMBHs (i.e. not in quasars) in the distant Universe.

APPENDIX

Since we consider only inactive galaxies as possible hosts of TDEs, the eROSITA count rate associated with their quiescent (non-flaring) state will likely be below the background level, which is estimated at 3.74×10^{-3} cts s^{-1} arcmin^{-2} in the 0.2–2 keV energy range (Merloni et al. 2012)[12]. This corresponds to 0.165 counts during a 240 s exposure inside the region of half-power diameter (HPD, 29") averaged over the FoV. Assuming Poisson distribution

[8] http://pan-starrs.ifa.hawaii.edu/public/home.html

[9] Wide-field Infrared Survey Explorer, http://irsa.ipac.caltech.edu/Missions/wise.html

[10] Such flares, if found by eRASS, may be interesting themselves for studying AGN variability mechanisms.

[11] Galaxy Evolution Explorer, http://www.galex.caltech.edu/

[12] This estimate includes the contributions of the cosmic X-ray background (CXB) and particle background, with the former dominating below 2 keV. Below 0.5 keV, a major contributor to the CXB is diffuse background emission from the Milky Way, whose intensity significantly ($\gtrsim$ 35%) varies over the sky (Lumb et al. 2002). This effect could be included in the real data analysis using the *ROSAT* map of the Local Hot Bubble emission (Snowden et al. 1997).

of the background counts, the probability for > 2 photons to be detected during this time inside HPD is $P_{bg} = 0.00066$, i.e. $< 10^{-3}$. Since we are looking for $\gtrsim 10$ times amplitude flares above the background level, the detection limit for the source in the bright phase corresponds to $2 \times 10 = 20$ counts inside the HPD region during 240 s. Therefore, the source count rate must exceed $C_{lim} = 0.167$ cts s^{-1} in the 0.2–2 keV energy band. The false rejection probability of $\sim 10^{-3}$ is sufficient for our purposes, since the resulting sample of TDEs is not expected to exceed a few thousand events.

Having 20 photons with energies from 0.2 to 2 keV inside the HPD region, it should also be possible to distinguish a soft X-ray spectrum as expected for a TDE flare from a harder spectrum typical of AGN. This distinction can be done in terms of a softness ratio, $SR = C_{0.4-1}/C_{1-2}$, the ratio of the count rates in the 0.4–1 keV and 1–2 keV energy bands. This ratio depends on the absorption column density N_H only weakly: for a power law spectrum with $\Gamma = 2$, $SR(N_H = 10^{20}$ cm$^{-2}) \simeq 1.9$ and $SR(N_H = 5 \times 10^{20}$ cm$^{-2}) \simeq 1.6$; for $\Gamma = 3$, $SR(N_H = 10^{20}$ cm$^{-2}) \simeq 4.0$ and $SR(N_H = 5 \times 10^{20}$ cm$^{-2}) \simeq 3.3$. Hence, having 20 counts within the HPD region and imposing the condition $SR > 2$, one can exclude at least $\sim 50\%$ of 'hard' ($\Gamma = 2$) sources but retain almost all 'soft' sources: for $\Gamma = 3$ and $N_H = 5 \times 10^{20}$ cm^{-2}, $SR > 2$ with $\simeq 80\%$ probability. Since a typical TDE signal is believed to be even softer ($\Gamma \simeq 5$ in the 0.4–2 keV energy band), only a tiny fraction of true TDEs will be missed if the criterion $SR > 2$ is used. In fact, one could use an extraction region several times larger than the HPD region if the accurate shape of the PSF is known. Combining counts with appropriate weights could increase the signal-to-noise ratio by a factor of $\sim \sqrt{2}$ and also the efficiency of the softness ratio criterion ($\sim 90\%$ of sources with $\Gamma = 3$ and $N_H = 5 \times 10^{20}$ cm^{-2} will be retained).

We also point out the possibility of exploiting the eROSITA sensitivity in the 2–10 keV energy range. For a source near the detection threshold, a 'soft' ($\Gamma = 3$ and $N_H = 5 \times 10^{20}$ cm^{-2}) spectrum will provide 0.30 cts in the HPD region in the 2–10 keV energy band for a 240 s exposure, whereas a 'hard' ($\Gamma = 2$ and $N_H = 5 \times 10^{20}$ cm^{-2}) spectrum will provide 1.12 cts. The hard (2–10 keV) eROSITA background is estimated at 0.04 cts in 240 s inside the HPD region (Merloni et al. 2012), although this number is rather uncertain due to the lack of data about the high energy particle environment near the L2 point, which is believed to determine the eROSITA background in this energy range. Thus, a non-zero flux in the 2–10 keV range is expected for $\gtrsim 1/2$ 'hard' sources with a 0.2–2 keV count rate near the detection limit mentioned above. This additional information can be used to distinguish TDE flares from e.g. AGN variability.

To summarize, we adopt a detection limit of 20 counts inside the HPD region during a 240 s exposure, i.e. $C_{lim} = 0.167$ cts s^{-1} in the 0.2–2 keV energy band. We propose $SR = C_{0.4-1}/C_{1-2} = 2$ as a boundary between 'soft' and 'hard' sources, which will allow one to retain as many as possible true candidates while rejecting a significant fraction of bogus ones. It might be necessary to slightly modify these flux and softness ratio criteria if the background level measured during the eRASS proves significantly different from the current estimates and/or typical TDE absorbing columns prove significantly different from the N_H value assumed above.

ACKNOWLEDGEMENTS

The research made use of grant NSh-5603.2012.2 from President of Russian Federation, RFBR grants 13-02-12250-ofi-m and 13-02-01365, programmes P-21 and OFN-17 of the Russian Academy of Sciences and grant 87019 from Ministry of Science and Education of Russian Federation. IK acknowledges the support of the Dynasty Foundation.

REFERENCES

Ayal S., Livio M., Piran T., 2000, ApJ, 545, 772
Alexander T., 2012, EPJWC, 39, 5001
Bower G. C., Metzger B. D., Cenko S. B., Silverman J. M., Bloom J. S., 2012, arXiv, arXiv:1210.0020
Brandt W. N., Hasinger G., 2005, ARA&A, 43, 827
Brockamp M., Baumgardt H., Kroupa P., 2011, MNRAS, 418, 1308
Burrows D. N., et al., 2011, Natur, 476, 421
Cappelluti N., et al., 2009, A&A, 495, L9
Carrasco L., Tovmassian H. M., Stepanian J. A., Chavushyan V. H., Erastova L. K., Valdés J. R., 1998, AJ, 115, 1717
Cenko S. B., et al., 2012, ApJ, 753, 77
Churazov E., Gilfanov M., Forman W., Jones C., 1996, ApJ, 471, 673
Donley, J. L., Brandt, W. N., Eracleous, M., & Boller, T. 2002, ApJ, 124, 1308
Dorman, B., & Arnaud, K. A. 2001, Astronomical Data Analysis Software and Systems X, 238, 415
Esquej, P., Saxton, R. D., Komossa, S., et al. 2008, A&A, 489, 543
Evans C. R., Kochanek C. S., 1989, ApJ, 346, L13
Gezari S., et al., 2009, ApJ, 698, 1367
Giannios D., Metzger B. D., 2011, MNRAS, 416, 2102
Greene J. E., Ho L. C., 2007, ApJ, 667, 131
Guillochon J., Ramirez-Ruiz E., 2013, ApJ, 767, 25
Gurzadian V. G., Ozernoi L. M., 1981, A&A, 95, 39
Halpern J. P., Gezari S., Komossa S., 2004, ApJ, 604, 572
Hills J. G., 1975, Natur, 254, 295
Ho, L. C. 2008, ARA&A, 46, 475
Hogg, D. W. 1999, arXiv:astro-ph/9905116
Hopkins P. F., Richards G. T., Hernquist L., 2007, ApJ, 654, 731
Kaiser N., et al., 2010, SPIE, 7733,
Kesden M., 2012, PhRvD, 86, 064026
Khabibullin I., Sazonov S., Sunyaev R., 2012, MNRAS, 426, 1819
Komatsu E., et al., 2011, ApJS, 192, 18
Komossa, S. 2002, Reviews in Modern Astronomy, 15, 27
Komossa S., Halpern J., Schartel N., Hasinger G., Santos-Lleo M., Predehl P., 2004, ApJ, 603, L17
Komossa S., 2012, AdAst, 2012
Kormendy J., Richstone D., 1995, ARA&A, 33, 581
Kormendy J., Ho L., 2001
Krolik J. H., Piran T., 2012, ApJ, 749, 92
Laguna P., Miller W. A., Zurek W. H., Davies M. B., 1993, ApJ, 410, L83
Lei W.-H., Zhang B., 2011, ApJ, 740, L27
Levan A. J., et al., 2011, Sci, 333, 199
Lidskii V. V., Ozernoi L. M., 1979, SvAL, 5, 16
Lin D., Carrasco E. R., Grupe D., Webb N. A., Barret D., Farrell S. A., 2011, ApJ, 738, 52

Lodato, G., King, A. R., & Pringle, J. E. 2009, MNRAS, 392, 332
Lumb D. H., Warwick R. S., Page M., De Luca A., 2002, A& A, 389, 93
MacLeod M., Guillochon J., Ramirez-Ruiz E., 2012, ApJ, 757, 134
Maksym W. P., Ulmer M. P., Eracleous M., 2010, ApJ, 722, 1035
Massaro F., D'Abrusco R., Ajello M., Grindlay J. E., Smith H. A., 2011, ApJ, 740, L48
Merloni A., et al., 2012, arXiv, arXiv:1209.3114
Metzger B. D., Giannios D., Mimica P., 2012, MNRAS, 420, 3528
Nikolajuk M., Walter R., 2013, arXiv, arXiv:1304.0397
Pavlinsky M., et al., 2012, SPIE Proc., in press
Peebles, P. J. E. 1993, Principles of Physical Cosmology by P.J.E. Peebles. Princeton University Press, 1993. ISBN: 978-0-691-01933-8
Phinney E. S., 1989, IAUS, 136, 543
Rees, M. J. 1988, Nature, 333, 523
Saxton R. D., Read A. M., Esquej P., Komossa S., Dougherty S., Rodriguez-Pascual P., Barrado D., 2012, A&A, 541, A106
SDSS-III Collaboration, et al., 2012, arXiv, arXiv:1207.7137
Sembay S., West R. G., 1993, MNRAS, 262, 141
Shakura, N. I., & Sunyaev, R. A. 1973, A&A, 24, 337
Snowden S. L., et al., 1997, ApJ, 485, 125
Stone N., Sari R., Loeb A., 2012, arXiv, arXiv:1210.3374
Strubbe, L. E., & Quataert, E. 2009, MNRAS, 400, 2070
Ulmer, A. 1999, ApJ, 514, 180
van Velzen S., et al., 2011, ApJ, 741, 73
van Velzen S., Körding E., Falcke H., 2011, MNRAS, 417, L51
van Velzen S., Frail D. A., Koerding E., Falcke H., 2012, arXiv, arXiv:1210.0022
Vaughan S., Edelson R., Warwick R. S., 2004, MNRAS, 349, L1
Veilleux S., Osterbrock D. E., 1987, ApJS, 63, 295
Wall, J. V., Jenkins, C. R., Ellis, R., et al. 2003, Practical statistics for astronomers, by J.V. Wall and C.R. Jenkins. Cambridge observing handbooks for research astronomers, vol. 3. Cambridge, UK: Cambridge University Press, 2003
Wang J., Merritt D., 2004, ApJ, 600, 149
Warwick R. S., Saxton R. D., Read A. M., 2012, A&A, 548, A99
Wright E. L., et al., 2010, AJ, 140, 1868